Vibration-Driven Self-Assembly in 4D Printing: From Spheres to Airfoils

Cooper Mendlinger[1]
University of Georgia, Athens, GA, 30602, United States

Ramana Pidaparti[2]
University of Georgia, Athens, GA, 30602, United States

The aerospace industry, motivated by the potential for next-generation travel, requires the exploration of supersonic vehicle designs and manufacturing. Despite this, the design processes for supersonic fighter jets like the F-15, F-22, and F-35 have remained largely unchanged, relying on established frameworks. As Industry 4.0 progresses across various sectors, including aerospace design, integrating AI into different stages of the design process holds the potential to revolutionize how new designs are conceived. With the increasing precision of large language models (LLMs) and other AI technologies, there is a significant opportunity to transform current methodologies for supersonic aircraft. The incorporation of LLMs and AI can redefine these starting points, altering the entire design process. This paper explores the application of LLMs and AI in the preliminary design of supersonic aircraft, focusing on their ability to analyze and optimize aerodynamic properties. By utilizing AI-driven tools and computational fluid dynamics (CFD) simulations within CAE software such as ANSYS Fluent, we aim to evaluate the performance of AI-generated designs compared to traditional, experimentally validated supersonic aircraft.

Nomenclature

(Nomenclature entries should have the units identified)

A = amplitude of oscillation
c = chord length
dt = time step
$F_{friction}$ = Force component of the friction acting on a piece with the shaker plate
F_{net} = Total Force component acting on the piece inflicted by the shaker table than initials movement
F_{vib} = Force component that is enacted on the pieces by the tables movement/striking the pieces.
h = height
m = mass
t = time
ω = angular frequency
V = Voltage
ϕ = phase shift

Subscripts

max = maximum of value
vib = vibration
friction = friction

1. Introduction

Self-assembly, a phenomenon ubiquitous in nature, is a process where a system spontaneously forms organized structures from pre-designed building blocks or components without external guidance. It describes the

1 Undergraduate Assistant, College of Engineering, DICE Lab, UGA, AIAA Number: 1799640, Undergraduate Student, email: cam03006@uga.edu
2 Professor, College of Engineering, 712B Boyd Research Center, and Associate Fellow

spontaneous organization of individual components into ordered structures driven by local interactions and minimal external intervention (Odum, 1988). This phenomenon is prevalent in nature, such as in the formation of microtubules from tubulin dimers, protein folding, formation of lipid bilayers in cell membranes, and the crystallization of snowflakes (Mitchison, 2021; Misteli, 2001). In biological systems, self-assembly often minimizes free energy, as seen in protein folding or DNA base pairing. Similarly, engineered systems can exploit external forces—such as vibrations—to navigate energy barriers and settle into low-energy states. In engineering, self-organization principles can be harnessed to create innovative manufacturing processes, particularly in the field of 4D printing.

4D printing is an advanced manufacturing technology that extends the capabilities of traditional 3D printing by incorporating the dimension of time ((Tibbits, 2017, Chu et al., 2020). Unlike traditional 3D printing, which produces static objects, 4D-printed objects can transform their shape or properties over time in response to external stimuli such as heat, moisture, light, pH, vibration or other mechanical energy. Chu et al., present several interesting applications and insights to emphasize the need for addressing challenges related to material selection, computations, and the need for innovative design strategies for manufacturing 4D technologies. Thus, 4D printing through the integration of smart materials and intelligent design allows 3D objects to adapt, self-assemble, and even self-repair, offering significant potential for various applications, including aerospace, construction, and soft robotics engineering. Demoly et al. (2021) and others make a case for 4D printing through self-assembly advanced manufacturing technologies in the Industry 4.0 applications.

The motivation for this work lies in its potential to revolutionize manufacturing processes, particularly for applications requiring precision and adaptability, such as aerospace components through 4D printing. Traditional assembly methods often rely on manual labor or complex robotics, which can be costly and time intensive. 4D printing through vibration-driven self-assembly (Sarma et al., 2023) offers a simpler, scalable alternative, using minimal energy input to achieve complex outcomes. This study leverages vibrational energy as a stimulus to orchestrate the self-assembly of 3D-printed components embedded with magnets. By employing a shaker table to impart controlled vibrations, we guide these components into stable configurations, mimicking natural systems where energy landscapes dictate structural stability.

The objective of this paper is to investigate the 4D printing concepts through a series of experiments transitioning from basic spherical shapes to aerodynamically critical airfoils, emphasizing the preservation of mechanical and functional properties. Through theoretical modeling and empirical validation, we aim to establish a framework for optimizing vibrational parameters and advancing 4D printing technology. The details of experiments, theoretical modeling and testing results are briefly presented in the next sections.

2. Experimental Setup

2.1 Materials and Fabrication

The experimental setup involves both fabrication of 3D printed design components along with small cylindrical magnets (smart material) to self-assemble under vibration stimuli (mechanical shaker). The details of the 3D components and their fabrication are briefly discussed below.

The components in this study were fabricated using polylactic acid (PLA) filament via fused deposition modeling (FDM), a widely accessible and cost-effective 3D printing technique. PLA was selected for its mechanical strength, ease of printing, and compatibility with embedded elements. Neodymium magnets (3×2 mm) were integrated into the components after the printing process via tolerance interference to enable magnetic interactions, serving as the primary mechanism for connection during self-assembly.

Sphere Components: The simplest geometry tested was a sphere with a 0.5-inch radius, assembled from eight identical 1/8th segments which is displayed in Figure 1. Each segment featured magnets at its interior corners, ensuring alignment and stability upon assembly. This design allowed us to establish baseline vibrational parameters in a symmetric, isotropic system.

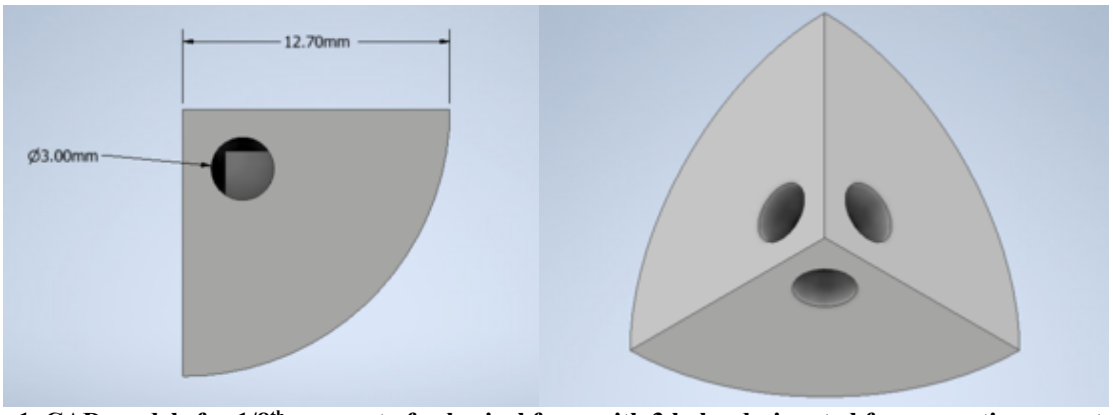

Fig 1. CAD models for 1/8th segment of spherical form with 3 holes designated for magnetic connectors

"UGA" Shape: A branded shape representing the University of Georgia logo was designed as an intermediate complexity test, though experimental results for this configuration are pending and will be explored in future work.

Airfoil Components: The most complex structure was a symmetrical S1016 airfoil and has a 5-inch chord length, assembled from six distinct components which is shown through the sectioning in Figure 2, which demonstrates how each unique component was constructed and dimensioned to accompany the magnetic bonding mechanism and convey the airfoil's shape. The airfoil's aerodynamic profile, inspired by NACA standards, required precise alignment to maintain lift and drag characteristics, posing a significant challenge for self-assembly.

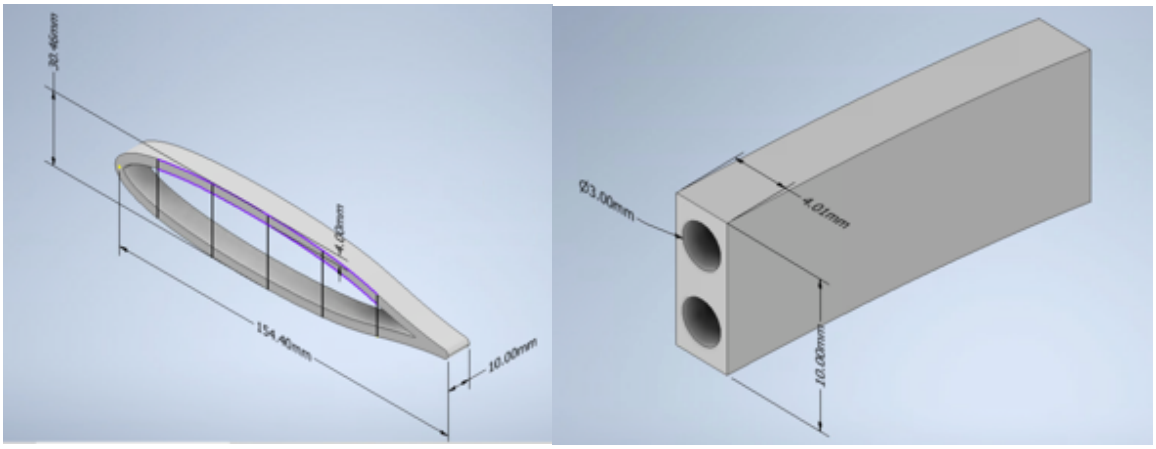

Fig 2. Complete S1016 Airfoil with sectioning separating unique shapes on the left and its connector mechanism dimensions on the right

The use of magnets introduces a dual-force system: vibrational energy drives motion, while magnetic attraction stabilizes connections. This interplay mimics natural systems where competing forces—such as van der Waals interactions and Brownian motion—govern assembly.

2.2 Shaker Table Configuration

Fig 3. Modal Shop Model 2075E with Mounting Inserts for Custom Attachments

A vibration device, The Modal Shop's Dual-Purpose Shaker Model 2075E provides up to 75 lbf pk sine force, shown in Figure 3. A large armature (3.25 in/8.3 cm diameter platform table served as the experimental platform, delivering controlled harmonic oscillations to the components. A custom mount was created featuring a 12-inch diameter circular platform with a 3-inch lip, which constrained component movement while allowing sufficient freedom for self-organization. Vibrational parameters were systematically varied to identify optimal conditions:

Sphere Tests: Amplitudes of 2V, 3V, and 4V paired with frequencies of 10Hz, 15Hz, and 20Hz.
Airfoil Tests: Amplitudes of 4V, 5V, and 6V paired with frequencies of 10Hz, 15Hz, and 20Hz.

The voltage settings correspond to the amplitude of oscillation, while frequency governs the rate of energy input. The containment lip minimized component loss during high-energy trials, enhancing the reliability of the assembly process. The testing parameters were chosen based on the theorical analysis of bonding mechanics for this system, which is discussed in the next section.

3. Theoretical Background,

The components, unattached to the shaker table, experience vibrational excitation as free bodies on a moving surface. The table's displacement is harmonic:

$$x_{table} = A\,sin(\omega t) \quad \text{Eq. (1).}$$

where A is amplitude (proportional to voltage), $\omega = 2\pi f$ is angular frequency, and
t, is time. Its acceleration, which given by the manufacture shown in Figure 4, can also be expressed by:

$$a_{table}(t) = -\omega^2\,A\,sin(\omega t) \quad \text{Eq. (2).}$$

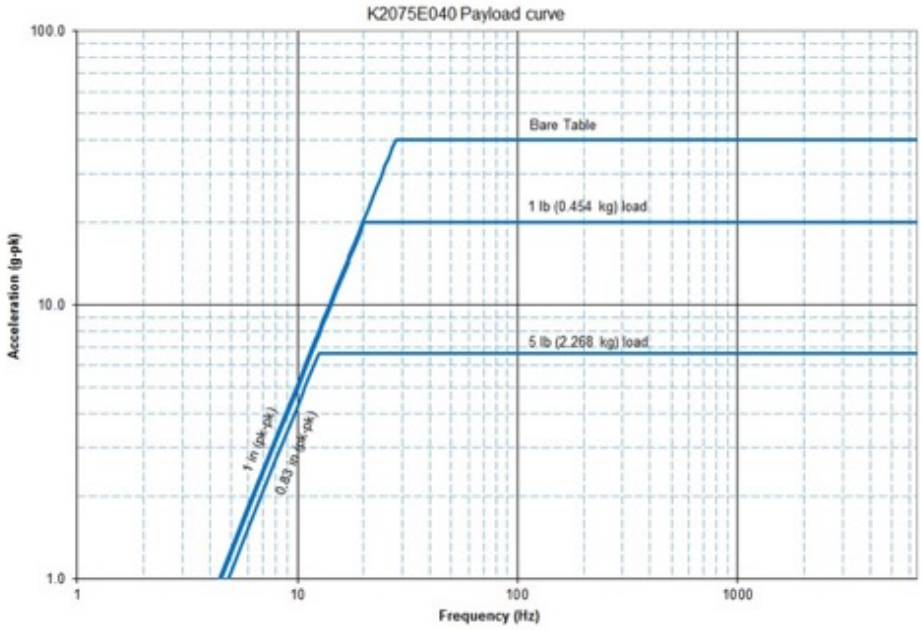

Fig 4. Payload Curve Displaying the acceleration of attachment with varying frequencies.

Since the pieces are not fixed, they slide or bounce on the table, influenced by this acceleration. The force imparted to a piece of mass, m arises from friction or intermittent contact, approximated as:

$$F_{vib}(t) = ma_{table}(t) = -m\omega^2 A sin(\omega t) \quad \text{Eq. (3).}$$

This force drives motion, with peak magnitude:

$$F_{vib,max} = m\omega^2 A \quad \text{Eq. (4).}$$

The displacement of a free piece, $x_{piece}(t)$, depends on its interaction with the table. Assuming sliding with friction (coefficient μ), the net force is:

$$F_{net}(t) = F_{vib}(t) - F_{friction} \quad \text{Eq. (5).}$$

where $F_{friction} = \mu mg$ (gravity g≈ 9.8 $\frac{m}{s^2}$) opposes motion when $||F_{vib}| > F_{friction}$ If $|F_{vib}| < F_{friction}$, the piece remains static. For simplicity, consider a piece in brief contact (e.g., bouncing), where its displacement lags the table's due to inertia and reconnects periodically. The relative displacement is complex, but we approximate its motion as:

$$x_{piece}(t) \approx A' sin(\omega t - \phi) \quad \text{Eq. (6).}$$

where A' < A accounts for energy loss (friction, collisions), and ϕ is a phase shift. The piece's acceleration aligns with a_{table} during contact, driving F_{vib}.

.

Bond Stability Analysis

Correct magnetic connections, with full pole overlap, yield $F_{mag} \approx$ 10N, while misaligned ones offer ~2–5 N. When $F_{vib,max} > F_{mag}$, weak bonds break, freeing pieces for reassembly. Polarity (P-N vs. P-P) rejects incompatible pairings, but stability under force filters configurations. Conducting the calculations suggests that the theorical range for breaking weak connecting pieces and sustaining correct connections hovers around 4.5V-5V with a frequency ranging around 15-20Hz. The poor connections show apparent instability from surface connections and flush connection sites that provide higher bonding forces. Like the fittings of active sites and substrates of enzymes, the contour of the complex curves of the airfoil provides very specific fittings to create the surface area of interaction between the magnets that have enough force to prevent disruption. The method of sectioning can be investigation to create more complex bonding site surfaces that can prevent unintended connections but can increase rate of bonding immensely as probability for correct interactions decreases.

4. Results and Discussion

4.1 Sphere Assembly Results

The sphere experiments provided a foundational understanding of vibrational self-assembly. At 2V and 10Hz, component mobility was limited, resulting in incomplete assembly due to insufficient energy to overcome initial misalignments, yielding no formation of any connections as the weight of each piece overpowered the seismic force

being imparted. Increasing the amplitude to 3V gained more consistent success, with segments forming semispherical shapes, displayed in the after section of Figure 5, within 30 seconds of the initial displacement. Finally, the greatest end of the selected range 4V, yielded the most promising results, as shown in Figure 6, as the higher displacements induced created more opportunities for collision and overcoming the increasing weight as the shapes combined. The higher amplitude enhanced collision frequency, while the moderate frequency prevented excessive disruption. At 20Hz, however, rapid oscillations prevented the shapes from receiving a greater impulse as they drop and the reconnected with the surface of the plate. The 15Hz frequency saw the most success in balancing increasing the rate of collisions without sacrificing the force acting on the shapes. Although there weren't complete spheres created the movement towards the optimal combination of amplitude and frequency shows coupled success in number of correct alignments. The spherical symmetry simplified alignment, making this a robust proof-of-concept for the methodology.

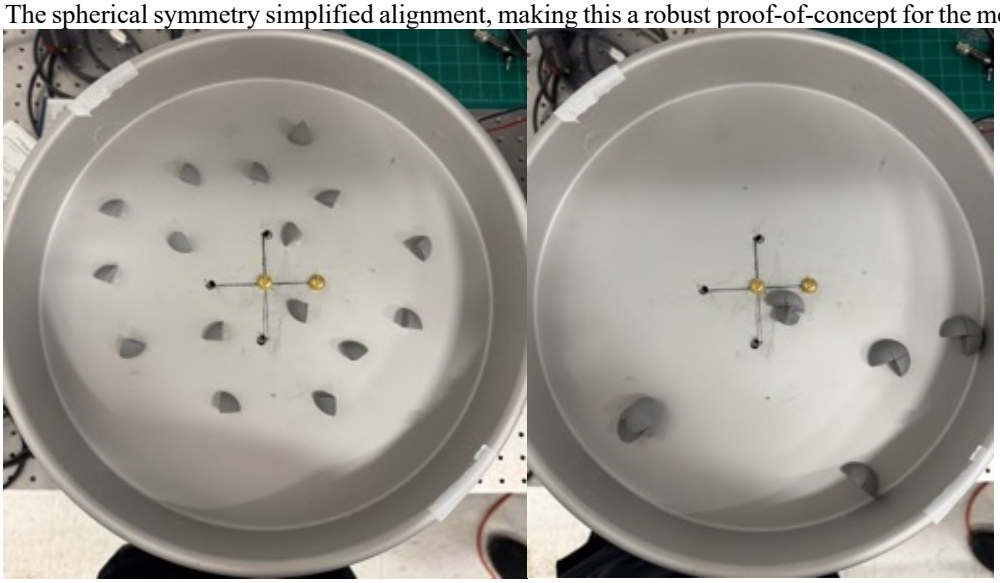

Fig 5. before and after of Shaker Test with Spherical Shapes at 3V and 10Hz

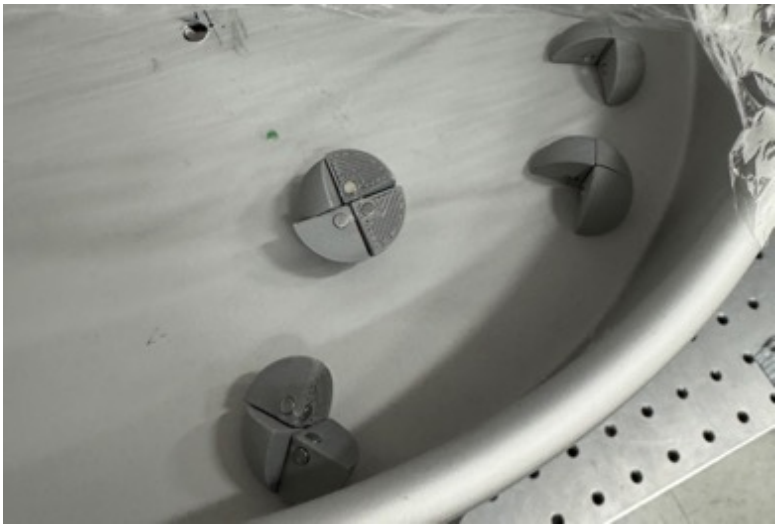

Fig 6. After of Shaker Test with Spherical Shapes at 4V and 15 Hz

4.2 Airfoil Assembly Results

The airfoil posed greater complexity due to its asymmetric geometry and functional requirements. At 4V and 10Hz, the components exhibited frequent movement, but often stalled in misaligned states due incorrect magnetic connections and the combined weight preventing the disruption of the bonds at this voltage. This produced not ideal configurations as shown in Figure 7, which showcased how the magnetic attraction creates unbiased connections if the forcing from the plate is not high enough to break it apart. The 5V, 15Hz configuration proved further successful,

achieving greater assembly with a higher rate of proper alignment of the S1016 profile. Figure 8 details the results from testing the highest amplitude (6V) and at both low and moderate frequency (10Hz and15Hz respectively) introduced the greatest result in achieving the profile with the leading edge having the upper and lower halves extending outwards towards the trailing edge while eliminating the pieces connecting perpendicularly with two other shapes.

Figure 7. Before and After Shaker Test with S1016 Airfoil segments at 4V and 10 Hz

Figure 8. After of Shaker Test with S1016 Airfoil Segments at 6V and 10 Hz on the left and 6V and 15 Hz on the right

Preserving the airfoil's shape was critical, as deviations could alter lift and drag coefficients as well as compromise structural integrity of the profile. Visual analysis confirmed that the 6V, 15Hz case moved towards a chord length within the target, 5 inches, with an inability to fully enclose the shape. This suggests that vibrational energy can be tuned to balance mobility and stability in complex systems but without the proper achieved amplitude will deviate from the intended shape or not form at all.

4.3 Stability and Energy Optimization

The containment lip played a pivotal role in maintaining component proximity, effectively reducing the energy required for assembly by preventing ejections. Stability followed an energy-bond analogy: stronger magnetic connections resisted disruption under lower vibrational forces, akin to covalent bonds in chemistry. The optimal

parameters minimized excess kinetic energy, ensuring that components settled into energy minima without overshooting.

Comparatively, the airfoil required higher amplitudes than the sphere due to its greater mass and shape complexity, highlighting the need for tailored energy inputs. These findings align with simulations predicting that stable configurations emerge when vibrational forcing aligns with the system's natural dynamics.

5. Future Work

Future experiments will expand to the "UGA" shape, testing the adaptability of the methodology to irregular geometries. Additional work will refine airfoil assembly by incorporating real-time feedback systems to dynamically adjust vibrational parameters. Scaling the process to larger structures and integrating multi-material components (e.g., flexible hinges) could further enhance 4D printing applications. These advancements will be documented at the AIAA Region II Conference in April 2025.

6. Conclusion

Experimental study was conducted to investigate the promise of 4D technology through self-assembly for simple structures including spheres and airfoils. This research furthers the validation vibration-driven self-assembly as a viable strategy for 4D printing, bridging bio-inspired principles with engineering innovation. By optimizing the stimuli, we can achieve progress towards stable assembly of complete spheres and airfoils, attempting to preserve structural and aerodynamic integrity. Theoretical models of harmonic motion and energy landscapes provided a mechanistic understanding, while experimental results demonstrated practical feasibility. The strength of magnetic bond and form/orientation producing geometric stability form the variables of structure that govern the assemblies that as the time period of interactions approaches infinity, will reach its most stable form i,e the correct configuration. The application to an S1016 airfoil underscores the potential for 4D printing in aerospace and beyond, offering a scalable, energy-efficient alternative to traditional manufacturing. Based on the preliminary results obtained it was shown it is feasible to adopt this 4D printing for future design applications including aerospace structural systems. However, further research and studies are needed to realize the potential of 4D printing.

Acknowledgements

The authors thank Dr. Ben Davis for his help and support in the experimental study.

References

[1] Airfoil Tools. (n.d.). *S1016-il - S1016 (s1016-il)*. Retrieved March 02, 2025, from http://airfoiltools.com/airfoil/details?airfoil=s1016-il

[2] Fre´de´ric Demoly et al. "The status, barriers, challenges, and future in design for 4D printing". In: *Materials & Design* 212 (2021), p. 110193.

[3] Honghui Chu et al. "4D printing: a review on recent progresses". In: *Micro-machines* 11.9 (2020), p. 796.

[4] Jackson, J. D., & Fox, R. F. (1999). Classical Electrodynamics, 3rd ed. *American Journal of Physics*, *67*(9), 841–842. https://doi.org/10.1119/1.19136

[5] Timothy J Mitchison and Christine M Field. "Self-organization of cellular units". In: *Annual review of cell and developmental biology* 37 (2021), p. 23.

[6] Tom Misteli. "The concept of self-organization in cellular architecture". In: *The Journal of cell biology* 155.2 (2001), p. 181.

[7] Howard T Odum. "Self-organization, transformity, and information". In: *Science* 242.4882 (1988), pp. 1132–1139.

[8] Sanjay Sarma, O.V., Ardoin, C., Ibrahim, I.M., Parasuraman, R., Pidaparti, R.M. (2023). Systems Design Concepts Mimicking Bio-inspired Self-assembly. In: Chakrabarti, A., Singh, V. (eds) Design in the Era of Industry 4.0, Volume 3. ICORD 2023. Smart Innovation, Systems and Technologies, vol 346. Springer, Singapore. https://doi.org/10.1007/978-981-99-0428-0_31

[9] Tibbits, S. (2017). The emergence of 4D printing. *TED Conference Proceedings*. Available at: https://www.ted.com/talks/skylar_tibbits_the_emergence_of_4d_printing